Seventh International Conference on Computational Fluid Dynamics (ICCFD7), Big Island, Hawaii, July 9-13, 2012

ICCFD7-3401

Numerical studies on the impact of equivalence ratio oscillations on lean premixed flame characteristics and emissions

C. Schrödinger*, C. O. Paschereit* and M. Oevermann**
Corresponding author: christina.schroedinger@tu-berlin.de

* Institut für Strömungsmechanik und Technische Akustik, TU Berlin, Germany
** Division of Combustion, Chalmers University of Technology, Gothenburg, Sweden

Abstract: In this work, the numerical investigation of laminar and turbulent one-dimensional lean premixed methane-air flames subject to equivalence ratio oscillations is presented. Harmonic perturbations at various frequencies and with various amplitudes are regarded and their influence on CO and NO emissions, heat release fluctuations, and burning velocity is evaluated. The results indicate a strong non-linear behavior of the flame response for high forcing amplitudes attributed partly to the extension into the stoichiometric and rich combustion regime and partly to non-linear effects imposed due to the interaction of burning velocity and equivalence ratio oscillations leading to non-sinusoidal oscillations at the flame front. Furthermore, the turbulent considerations expose decreasing mean burning velocities and heat release rates with increasing amplitudes due to damping of turbulent fluctuations induced by the oscillations.

Keywords: Linear Eddy Model, Turbulence Modeling, Combustion, Variations in equivalence ratio, Heat release rate, Burning velocity, Emissions.

1 Introduction

Lean premixed combustion is used in gas turbine processes being able to operate under moderate temperatures and reduce emissions, such as NO_x and CO. A major drawback of lean premixed flames, especially when turbulent, is their susceptibility to combustion instabilities. These instabilities may be driven by various effects and their interaction [1], thereunder coherent flow structures [2, 3], flame surface variation [4] and equivalence ratio fluctuations [5, 6].

Equivalence ratio fluctuations occur due to the unmixedness of fuel and air mass flows at the injection point of fuel. Variations in the fuel/air mixture arriving at the flame front lead to heat release fluctuations and were detected by Lieuwen et al. as one of the major causes for combustion instabilities at lean conditions [5, 6]. This is due to the relationship between equivalence ratio and chemical reaction time. The gradient of chemical reaction time and equivalence ratio increases significantly for premixed flames getting leaner. Moreover the chemical reaction time is inversely proportional to the reaction rate at lean conditions which amplifies the susceptibility to combustion instabilities.

Several works deal with the investigation of the flame response subject to variations in mixture composition. Numerical investigations of premixed laminar and counterflow flames [7, 8, 9, 10, 11, 12] as well as computational and experimental studies on bluff-body and swirl flames undergoing equivalence ratio variations [13, 14, 15, 16] have been performed. Furthermore the influence of strain effects/temporal strain rate fluctuations on diffusion flames have been studied [17, 18, 19].

Sankaran et al. [7] investigated unsteady methane-air flames in an opposed-flow configuration subjected to time-varying composition fluctuations. They concentrated on the determination of the dynamic flammability limit and found that the flammability region is extended to lower equivalence ratios as the frequency of oscillation is increased [12] while the mean equivalence ratio and temperature must be maintained higher

than the critical value for steady flammability limit. Analysis of the flame response to equivalence ratio fluctuations in terms of the flame transfer function [8, 10] showed that the heat release response is controlled by superposition of three disturbances: heat of reaction, flame speed, flame area. The influence of the particular disturbances varies with the oscillation frequency. Studies on the non-linearity of the heat release response identified two key mechanism [10]: the flame-kinematic mechanism driven by fluctuations in flame position associated with oscillations in flame speed [14] and a mechanism due to intrinsically non-linear dependence of flame speed and heat of reaction on equivalence ratio oscillations which is especially pronounce for composition fluctuations varying between lean and rich values.

König et al. [9] considered the response of laminar stretched premixed methane-air counterflow flames to periodical perturbations of mixture composition and inflow and observed that perturbations reach the flame only under certain conditions. The amplitude of perturbation reaching the flame decreases with increasing frequency due to dissipative processes and might even be completely leveled to a mean value before the flame zone. They further stated that perturbation do not qualitatively influence the behavior of chemical kinetics.

Strained laminar premixed counterflow flames were numerically studied by Richardson et al. and Rhou et al. [11, 12]. They regarded the effect of equivalence ratio gradients and fluctuations. They found that back/front supported flames propagate faster/slower than their premixed counterparts. Moreover the stratified flame propagation was determined in terms of displacement speed of the mixture. Richardson et al. [11] explain that reaction, diffusion and cross-dissipation components contribute to the displacement speed. Diffusion is thereby directly affected by strain responding most rapidly to strain variations whereas the reaction and cross-dissipation components' response is governed by flow and flame time-scales. Rhou et al. [12] further state that under lean conditions the propagation is dominated by diffusion of heat and under rich conditions by diffusion of several major species.

The non-linear response of bluff-body respectively swirl-stabilized flames were investigated experimentally by Balachandran et al. [13, 15] and Kim et al. [16]. Balachandran et al. found that the flame response depends on the strength of swirl [13] and the acoustic and convective compactness of the flame [15]. For compact flames (low frequencies) the heat release fluctuations mainly depend on equivalence ratio variations whereas for higher frequencies the heat release is dominated by the flame-vortex interaction. Kim et al. [16] state that the non-linear response becomes more pronounced with increasing modulation frequencies and decreasing equivalence ratios. Besides the phase between heat release and equivalence ratio oscillations increases linearly with frequency. Birbaud et al. [13] simulated a V-flame subjected to equivalence ratio fluctuations. The flame featuring wrinkles may interact with the fresh mixture for sufficient large wrinkling amplitudes generating a non-linear heat release response. Furthermore high levels of modulation induce velocity perturbation which in turn interact with the flame and modify its response.

Studying the influence of strain variation on diffusion flames Barlow et al. [17] detected that periodic variations in scalar dissipation rate show minor influence on species mass fraction while sudden decrease in scalar dissipation rate leads to an overshoot in OH and CO. Im et al. [18] found that NO_x and OH decrease with scalar dissipation and CO increases to a certain point near extinction. NO_x exhibits an increasing phase lag for increasing amplitude of fluctuation. 1D numerical computations on the effect of characteristic times of vortex on prompt and thermal NO formation paths showed that thermal NO is strongly dependent on the time history and not only on the particular dissipation rate whereas prompt NO is almost independent of the time history and only depends on certain values of the dissipation rate [19].

In the present work, we numerically investigate the influence of periodic equivalence ratio oscillations on lean, premixed flames that are strongly turbulent using detailed chemistry. We further compare the results to laminar flames under the same conditions and evaluate pollutant formations of NO_x and CO, heat release rate fluctuations, and species displacement speeds. The benefit of the turbulent approach used for the simulations is that the influence of small scale turbulence is regarded additional to large scale stratification. The numerical method utilized for the studies is the one dimensional Linear Eddy Model [20, 21]. This model resolves all relevant physical and chemical length and time scales and is therefore applicable to the whole range of combustion regimes which can be characterized by the Borghi-Diagram [22]. Gas turbine combustors normally operate in the high turbulent torn flame fronts regime where small scale eddies play an important role. This regime is captured by the Linear Eddy Model making it advantageous to many other combustion models. The Linear Eddy Model can be understood as one-dimensional DNS but due to its one-dimensionality it is computationally much more efficient. Parametric studies are thus feasible. The flame response is determined for a large range of reasonable oscillation frequencies and amplitudes.

The paper is organized as follows. First the numerical setup is described (Sec. 2). The Linear Eddy Model, the code implementation and the underlying combustion mechanism are explained in detail. In the results section (Sec. 3) the differences of turbulent and laminar flames are emphasized before the response of the flame on the fluctuations in mixture composition are characterized by emissions of CO and NO, heat release rate and displacement speeds.

2 Numerical methods

2.1 The Linear Eddy Model

The Linear Eddy Model (LEM) developed by Kerstein [20, 21] resolves all physically relevant length (for turbulent flows: Kolmogorov scale, η, to integral length scale, L) and time scales on a one-dimensional domain. The main idea behind this approach is to treat molecular diffusion processes and turbulent advection separately. Molecular diffusion is implemented deterministically whereas turbulent stirring is represented by a sequence of statistically independent rearrangement events. The rearrangement events can be regarded as the one dimensional analog of turbulent eddies. They are expressed by triplet maps, which compress the scalar field within a chosen segment by a factor of three and the original field is then replaced with three adjacent copies of the compressed field, with the middle copy spatially inverted (Fig. 1). The maps are

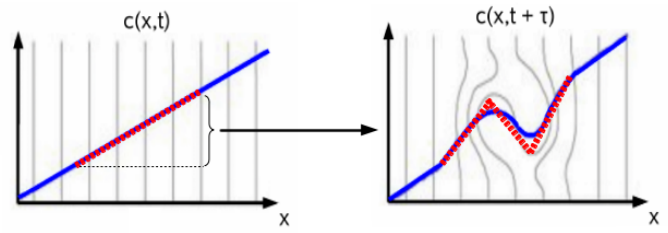

Figure 1: Triplet Map applied to a scalar gradient c(x,t)

measure preserving and do not introduce discontinuities into the scalar profiles. Each event is governed by three random variables: the time when the eddy occurs, the location and the size of the eddy. The location is chosen randomly. The size of the eddy is chosen from a distribution of domain sizes which is obtained by applying Kolmogorov scaling laws. Identifying that the rearrangement events induce a random walk of one particle on a line, a rate parameter, λ, with dimensions $[l^{-1}t^{-1}]$ and a pdf describing the length distribution, $f(l)$, can be determined. The diffusivity of the random walk is thereby interpreted as the turbulent diffusivity D_t:

$$\lambda = \frac{54}{5} D_t L^{-3} \frac{\left[1 - (\eta/L)^{-5/3}\right]}{\left[(\eta/L)^{4/3} - 1\right]}, \tag{1}$$

$$f_1(l) = \frac{-5/3}{L^{-5/3} - \eta^{-5/3}} l^{-8/3}. \tag{2}$$

The eddy occurence time is calculated from a Poisson process.

$$f_2(t) = \frac{1}{\tau} \exp -t/\tau, \tag{3}$$

where τ denotes the mean eddy occurrence time $< t >= \tau = \frac{1}{\lambda S}$ with S being the size of the one-dimensional domain. Considering Equ. 1, 2, and 3 three input parameters are needed for the model, namely the integral length scale L, the Kolmogorov scale η, and the turbulent diffusivity D_t. η and D_t can be derived from the turbulence intensity and the integral length using the relations $\eta = C_\eta L Re_t^{-3/4}$ and $D_t = {u'L}/{C_\lambda}$; Re_t is thereby the turbulent Reynolds number and C_η and C_λ are constants determined for a wide range of

turbulent premixed flames in [23]. The one-dimensional line of the Linear Eddy Model can be considered as a line of sight through a three-dimensional turbulent domain. In the case of premixed combustion the Linear Eddy domain represents a statistical cut perpendicular to a three-dimensional turbulent flame front.

The LEM reproduces important key features of turbulent mixing [21] and proved itself to be a valid model in studies on various research fields, amongst them LEM simulations on turbulent premixed combustion and pollutant formation by Menon et al. [23, 24].

2.2 Code implementation

The code is based on an implementation developed by Lignell et al. [25] for diffusion flames and One Dimensional Turbulence (ODT) [26], which is closely related to LEM, but also considers velocities. The code was refined to be suitable for one-dimensional turbulent premixed flames employing the Linear Eddy Model. In the following the code implementation will be described in detail.

2.2.1 Diffusive advancement

The diffusive advancement is implemented using a Lagrangian formulation. This implies no mass fluxes across the cell boundaries which leads to expansion and contraction of cells. The Lagrangian formulation treats 1D advection originating from dilatation in variable density flows implicitly. This is a huge advantage over an Eulerian formulation since the dilatation velocity is generally much larger than diffusion velocities. The Eulerian formulation is therefore controlled by the advection process causing very small advancement time steps. The Lagrangian formulation in contrast is controlled by the diffusion process allowing for larger advancement time steps.

In the following the Lagrangian transport equations will be presented for mass, species, and energy. $\mathcal{S}$ denotes the Lagrangian system containing a fixed mass of fluid or species without any mass crossing the system boundaries $\partial\mathcal{S}$. The quantities are generally evaluated at the cell center. Flux terms or other quantities given at the cell faces are labeled with subscripts fl and fr for left and right cell faces, respectively. For discretization of spatial derivatives central differences are used.

The pressure equation will not be described as in the current work the pressure is assumed constant in space and in time. For detailed derivation of the transport equations we refer to [25].

Continuity equation

The Lagrangian formulation of the continuity equation reads

$$\frac{d}{dt}\int_{\mathcal{S}} \rho dV = 0. \tag{4}$$

In 1D and with constant properties in the control volume Equ. 4 becomes

$$\frac{d}{dt}(\rho\Delta x) = 0, \quad \rightarrow \quad \rho\Delta x = const.. \tag{5}$$

Species equation

The Lagrangian conservation equation for a diffusing species α is given given by

$$\frac{d}{dt}\int_{\mathcal{S}} \rho Y_\alpha dV = \frac{d}{dt}\int_{\mathcal{S}} \omega_\alpha dV, \tag{6}$$

where Y is the mass fraction and ω is the reaction rate. Considering the Reynolds transport theorem and Equ. 5 and assuming uniform properties in the control volume, Equ. 6 can be rewritten as

$$\frac{dY_\alpha}{dt} = -\frac{1}{\Delta x}(j_{\alpha,\mathrm{fr}} - j_{\alpha,\mathrm{fl}}) + \frac{\omega_\alpha}{\rho}. \tag{7}$$

$j_\alpha = \rho Y_\alpha v_\alpha^D$ denotes the diffusive flux, where v_α^D is the species diffusion velocity. The diffusive flux of species α is expressed by a variation of Fick's law:

$$j_\alpha = -\rho D_\alpha \frac{dY_\alpha}{dx} - \frac{\rho D_\alpha Y_\alpha}{M}\frac{dM}{dx}, \tag{8}$$

where D_α is the species diffusion coefficient and M is the mean molecular weight.

Energy equation

The energy equation for internal energy e in Lagrangian formulation is

$$\frac{d}{dt}\int_{\mathcal{S}} \rho e dV = \dot{Q} + \dot{W} = -\int_{\partial\mathcal{S}} \mathbf{q}\cdot\mathbf{n} dA - \int_{\partial\mathcal{S}} \mathbf{F}\cdot\mathbf{v}_{\text{sys}} dA, \tag{9}$$

where $\mathbf{q}$ is the heat flux vector, $\mathbf{F}$ is the surface force per unit area, $\mathbf{n}$ is the normal vector, and $\mathbf{v}_{\text{sys}}$ is the system velocity vector. Assuming pressure work as the only surface force, integration over the 1D control volume gives

$$\frac{de}{dt} = -\frac{1}{\rho\Delta x}(q_{\text{fr}} - q_{\text{fl}}) - \frac{P}{\rho\Delta x}(U_{\text{fr}} - U_{\text{fl}}). \tag{10}$$

U denotes the dilatational velocity and P the pressure, which is uniform in the control volume. Substituting e with enthalpy $h = e - P/\rho$ and rearranging yields

$$\rho\Delta x\frac{dh}{dt} = -(q_{\text{fr}} - q_{\text{fl}}) + \Delta x\frac{dP}{dt} + \underbrace{P\frac{d\Delta x}{dt} - P(U_{\text{fr}} - U_{\text{fl}})}_{=0}, \tag{11}$$

$$\frac{dh}{dt} = -\frac{1}{\rho\Delta x}(q_{\text{fr}} - q_{\text{fl}}) + \frac{1}{\rho}\frac{dP}{dt}. \tag{12}$$

The heat flux vector is of the form of Fourier's law:

$$q = -\lambda\frac{dT}{dx} + \sum_\alpha h_\alpha j_\alpha. \tag{13}$$

It includes thermal conduction (λ is the conductivity) and species mass flux.

2.2.2 Time integration

The solution of the ordinary differential equations in time are treated seperately. The enthalpy equation is solved explicitly using a first-order Euler method while the species equation is solved implicitly. Therefore, the species equation is splitted using the Strang-splitting method. The diffusive term of the species equation (Equ. 7) is solved in the first splitting step for $\Delta t/2$. Then the source/reactive term is solved in the second step for Δt and in the third step the diffusive term is again solved for $\Delta t/2$. Since the solution with detailed chemistry is usually stiff which causes the necessity of very small time steps for explicit treatment, implicit integration of the chemical source term is used. The integration is performed with CVODE [27]. In premixed combustion the diffusion turns out to be quite stiff as well. Hence, this part is integrated implicitly using the Thomas Algorithm, also known as tridiagonal matrix algorithm (TDMA).

The overall solution procedure for the diffusive advancement for one time step ($t_n \rightarrow t_{n+1}$) can be summarized in the following steps:

1. Calculation of fluxes (mass j, heat q).
2. Advancement of species equation using Strang splitting to obtain Y_α at t_{n+1}.
3. Advancement of energy equation to obtain h at t_{n+1}.
4. Calculation of M and T from Y_α and h at t_{n+1}.
5. Solving of the ideal gas law to obtain ρ at t_{n+1}.
6. Solving of Equ. 5 ($(\rho\Delta x)_{n+1} = (\rho\Delta x)_n$) to obtain Δx at t_{n+1}.

The solution procedure including molecular diffusion and turbulent stirring (triplet mapping) for the case of premixed combustion with outflow boundary conditions (Neumann boundary condition) is implemented such that

1. the eddy time, position and size are computed,
2. the eddy/triplet map is applied,
3. diffusion is updated to the eddy time and
4. eventually the domain is shifted so that the flame remains at the same position.

When shifting the LEM domain a new cell at the inflow side is created with predefined inflow properties. The outflow side is cut off to conserve the original domain size. The shifting length is calculated from the displacement speed which is determined for each species α from [28]

$$s_D = \frac{1}{\rho_u(Y_{\alpha,b} - Y_{\alpha,u})} M_\alpha \int \omega_\alpha dx \tag{14}$$

Indices u and b denote the unburnt and burnt states.

2.2.3 Mesh adaption

The Linear Eddy domain is descretizised on a non-uniform mesh. The domain $[0, S]$ consists of n cells with cell faces $x_{f,i}$ and cell centers x_i, where $x_{f,1} = 0$ and $x_{f,n+1} = S$ (domain length). The property profiles are assumed uniform in each cell. The number of cells varies due to the triplet mapping and mesh adaption procedures. By applying a triplet map the number of grid points for the regarded region is tripled. As this may imply an inappropriate discretization for the property profiles, very small cells which could impose stringent time-step constraints or large size ratios of adjacent cells, mesh adaption of this region has to be applied. On the other hand diffusive evolution necessitates mesh adaption. Diffusive advancement smooths property gradients that might lead to an over-resolved field. Furthermore, solving for reactive flows (regarding a scalar source term) may produce increased gradients and in combination with the Lagrangian formulation of the equation system this may result in expanded or contracted cell sizes.

The mesh adaption is performed by splitting or merging cells conserving mass. It is based on one or more property profiles, in the current work it is based on the temperature profile. The adaption of the profiles follows several rules explained hereafter. The cell size should not be larger, respectively smaller than a given maximum, respectively minimum cell size. The cell size is further bound to minimum and maximum gradients and curvatures which are also predefined. Eventually, a cell should feature a cell size ratio of less than 2.5 to its adjacent cells. The last constraint prevents irregularities in the mesh which could affect the accuracy of the diffusive process. For further information on the choice of the factor 2.5 we refer to [25].

The benefit of the adaptive-mesh implementation is the strong reduction of the number of grid cells needed to discretize a given domain with large gradients due to reaction and turbulent eddies.

2.3 Combustion mechanism

Detailed combustion mechanisms are necessary to investigate dynamic processes in combustion, especially regarding intermediate species such as pollutants NO_x and CO. The GRI-Mech 3.0 [29] is a standard mechanism for natural gas and ignition processes which has been validated against a huge number of data sets but turns out to be relatively slow regarding spatial and temporal resolved calculations as it consists of 325 reaction equations and involves 53 species. For these kind of computations smaller mechanisms have to be employed.

The combustion mechanism used in this work is a reduced mechanism derived from the GRI-Mech 3.0. The mechanism was developed within our working group for lean methane-air combustion at atmospheric conditions including NO_x- and CO-formation. All important NO_x-formation pathways for lean combustion were remained from the original mechanism. These are the thermal path, the N_2O-path, and the NNH-path. The the prompt(CH)-path has been neglected since its influence in lean premixed combustion up to an equivalence ratio of 0.95 is insignificant. Some adaption of reaction rates, more precisely pre-exponential factors of the Arrhenius equation, have been conducted to comply with the original mechanism. The reduced

mechanism consists of 23 species and 76 reactions. Several 1D test cases were run and in average the reduced mechanism was found to be more than 5 times faster than the GRI-Mech 3.0 regarding CPU time.

Figure 2 shows the validation of the reduced mechanism against the GRI-Mech 3.0. Mass fractions of CO and NO, computed from a reactor network with a zero-dimensional reactor with constant mixture composition inflow and volume outflow conditions, are compared for lean conditions. Furthermore temperature profiles and laminar burning velocities calculated for one-dimensional laminar flames are displayed. The agreement of the reduced with the original mechanism is overall very good. The burning velocities further compare satisfactory with a burning velocity model for methane-air flames by Abu-Orf [30].

The software Cantera [31] is employed to solve for thermodynamics, chemical kinetics and transport processes. Transport properties are determined using the mixture-averaged model.

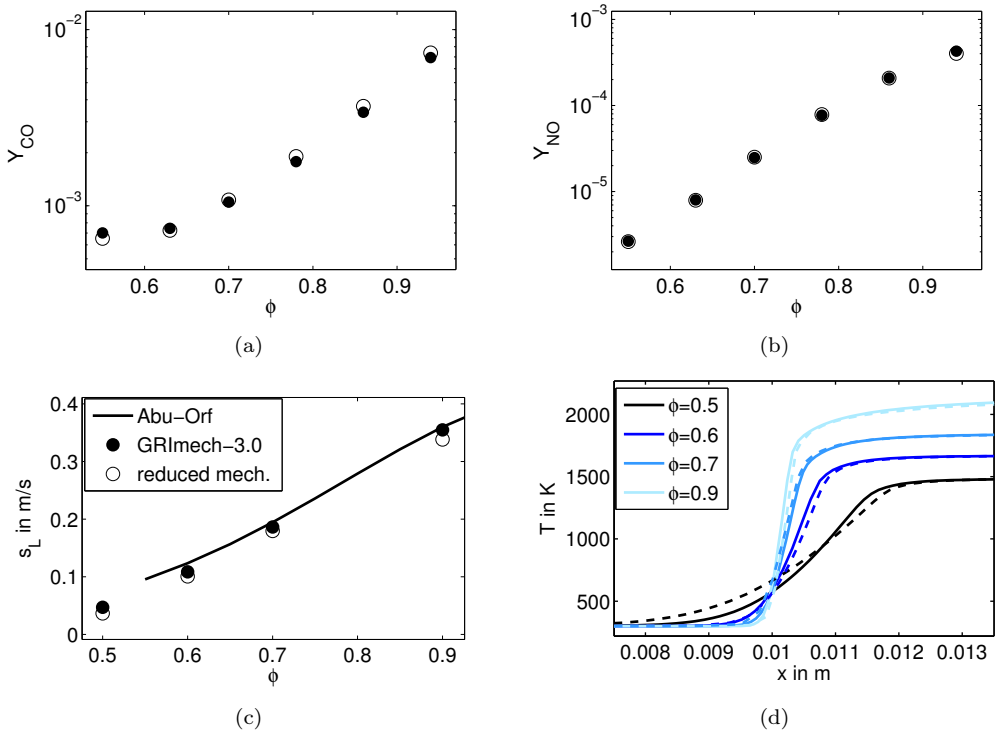

Figure 2: Validation of the considered reduced mechanism. (a) CO mass fraction vs. equivalence ratio; (b) NO mass fraction vs. equivalence ratio; (c) burning velocity vs. equivalence ratio in comparison with a correlation for laminar burning velocities of methane-air combustion by Abu-Orf [30]; (d) temperature profiles for different equivalence ratios for a one-dimensional laminar flame.

3 Results

3.1 Laminar vs. turbulent, constant equivalence ratio

One-dimensional simulations for the current studies have been performed for laminar and turbulent cases. A methane-air mixture with an equivalence ratio of 0.6 preheated to 425 K is investigated. The Kolmogorov and integral lengths for the Linear Eddy Model were taken from measurements in a combustion test rig; their values are 1e-4 m and 0.025 m, respectively. The turbulent diffusivity D_t was determined from the relation $D_t = {}^{u'L}/_{C_\lambda}$, with $u' = 10\,\mathrm{m/s}$. The constant C_λ is taken to be 15 which lead to good results for similar flames in previous studies [23]. Figure 3 shows the comparison of the laminar and turbulent flames. Mean temperature, heat release rates, CO-, NO- and NO_2- mass fraction profiles are given. Furthermore an instantaneous temperature profile for the turbulent case is presented. It clearly demonstrates that the turbulent flame features characteristics of distributed (eddy size $<$ laminar flame thickness) as well as flamelet (eddy size $>$ laminar flame thickness) combustion regimes. The mean profiles show the difference in flame respectively reaction zone extent which leads to an decrease of NO_x emissions, an increase of overall heat release rate and burning velocity for the turbulent flame. Due to a thicker flame the equilibrium state is reached later for the turbulent flame. The burning velocities are in average 0.22 m/s for the laminar case and 1.7 m/s for the turbulent case. The Linear Eddy Model thus predicts realistic turbulent burning velocities. The strong increase in burning velocity for the turbulent case is due to the interaction of small scale turbulence with the flame. This also causes the broadening of the flame. In addition eddies which are larger than the flame thickness imply the formation of hot pockets within the cold surrounding and additionally increase the burning velocity and heat release rate.

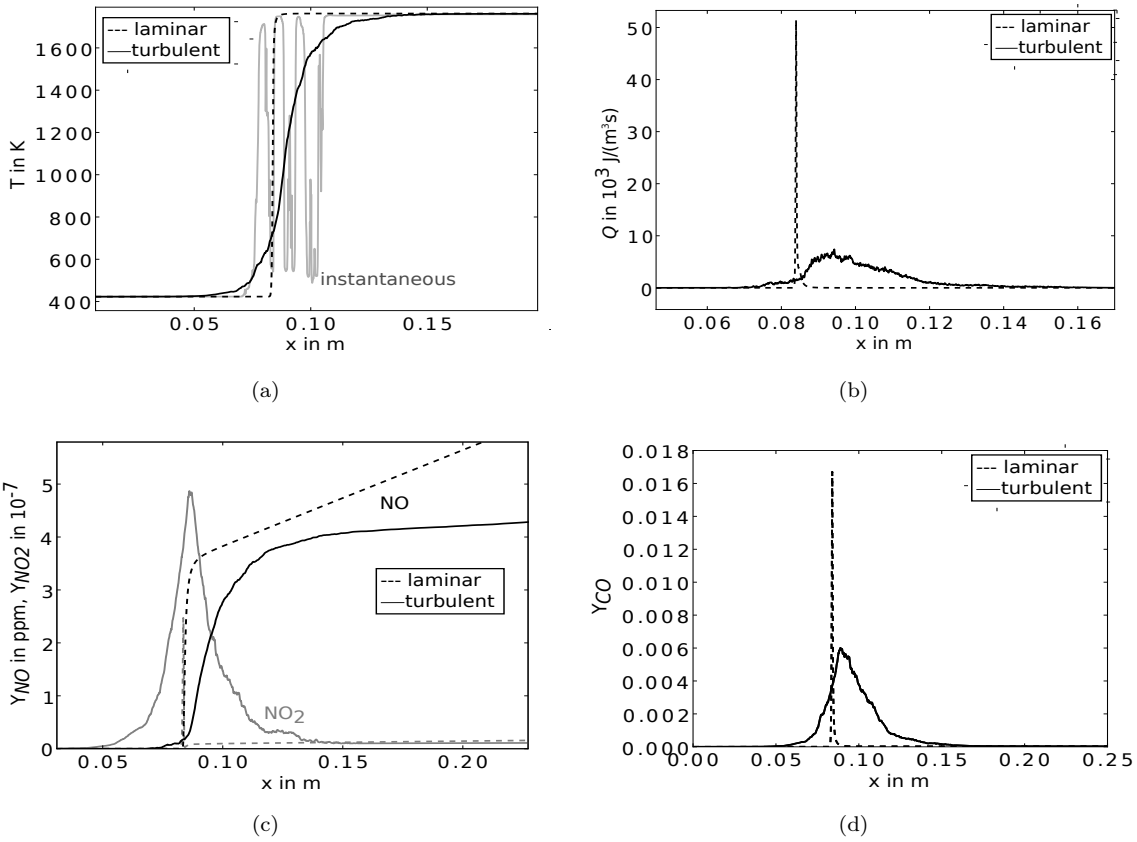

Figure 3: Comparison of laminar and turbulent one-dimensional flames. (a) Mean laminar and turbulent, and instantaneous turbulent temperature; (b) mean heat release rate; (c) mean NO- and NO_2-mass fraction; (d) mean CO-mass fraction.

3.2 Equivalence ratio oscillations

In this paper we concentrate on the investigation of equivalence ratio oscillations as they may occur in gas turbines under combustion instabilities. The methane mass fraction at the inflow side of the domain is set to a sinusoidal oscillation at constant temperature. The simulations are conducted for a frequency range of 20 Hz to 150 Hz and the amplitudes are varied in a wide range for representative frequencies. The computational domain has a length of 0.25 m for turbulent as well as laminar simulations. The flame was initially located at 0.02 m and 0.07 m for the laminar and turbulent cases respectively. The inflow velocity to shift the flame and keep it at the same position was set to the average displacement speed of the products, H_2O and CO_2, at each time step. The displacement speed of the products was chosen as it represents the burning velocity quite accurate. Considering the reactants, O_2 and CH_4, would cause too strong oscillations in the shifting speed and intermediates such as NO tend to be delaying and might show characteristics differing from that of the burning velocity when forced. Note that this approach leads to variations in the mass flow and causes an interaction of equivalence ratio oscillations and shifting speed. On the other hand this procedure allows for a more or less constant flame location within the domain. All simulations were run for 1 s to obtain enough periods of oscillation for averaging.

The relationship between equivalence ratio and dissipation rate for laminar realizations is given in Fig. 4. The dissipation rate χ is calculated from the mixture fraction ξ:

$$\chi = 2D(\mathrm{grad}\,\xi)^2, \tag{15}$$

where D denotes the thermal diffusivity. χ can be interpreted as the inverse of a characteristic diffusion time scale, imposed by the mixing field [32]. The phase averaged dependence of dissipation rate fluctuations on the equivalence ratio oscillation is plotted for the laminar simulations for three different relative perturbation amplitudes, 0.16, 0.50, and 0.83, for a forcing frequency of 90 Hz (Fig. 4(a)) and different forcing frequencies, 30 Hz, 60 Hz, and 120 Hz, at a relative perturbation amplitude of 0.66 (Fig. 4(b)), all at a position of 2 mm downstream of the inlet. All curves feature an eight-like shape which is attributed to the quadratic dependence of the dissipation rate on the mixture fraction gradient. It can be observed that the dissipation rate grows strongly with forcing amplitude and also with frequency. The frequency plot further shows that 2 mm downstream of the inlet the amplitude in the equivalence ratio is already decreased, the stronger the higher the frequency. For the simulations the described characteristics generally imply that the forcing amplitudes imposed at the inlet will not reach the flame. The higher the frequency the higher the diffusive processes and the lower the amplitude of oscillation at the flame front. For turbulent flows the dissipation is stronger than for laminar flows since turbulent mixing processes are superposed on the laminar processes, i.e. molecular diffusion. In the following the relative forcing amplitudes are always given with their values at the inlet of the simulation domain.

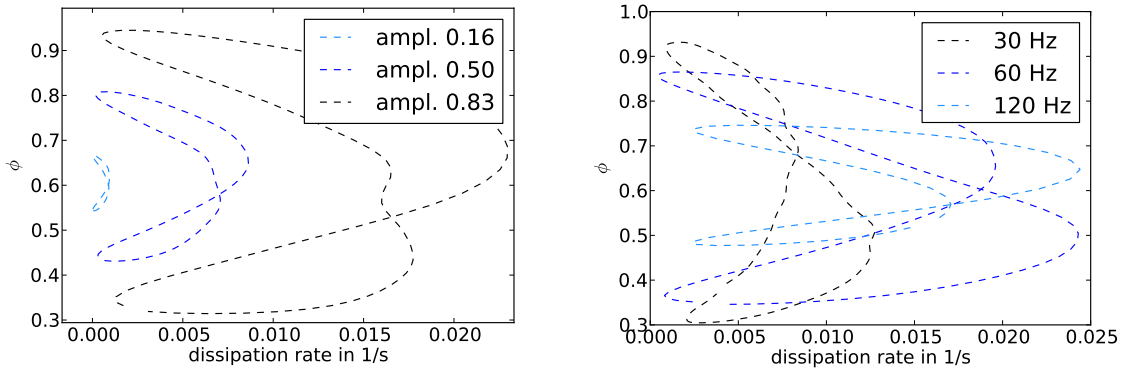

(a) (b)

Figure 4: Phase averaged relation between dissipation rate fluctuations and equivalence ratio oscillations 2 mm downstream of the inlet, laminar. (a) Variation of relative forcing amplitudes at 90 Hz; (b) variation of forcing frequency at constant amplitude of 0.66.

3.3 Influence of equivalence ratio oscillations on emissions of NO and CO

The emissions of NO and CO underlie strict regulations in modern gas turbine processes. It is therefore very important being able to control the emissions and to estimate their behavior under unsteady conditions. The qualitative (steady-state) behavior of NO and CO in dependence on the equivalence ratio is given in Fig. 5. The present studies concentrate on the lean combustion regime where modern gas turbines operate due to coexistent low NO and CO emissions. Both pollutants exhibit a nearly exponential growth with increasing equivalence ratio in the lean region. NO reaches its maximum close to stoichiometric conditions and decreases in the rich region whereas CO further increases. In the very lean combustion regime CO growth again due to quenching effects. Important for the present studies is to note that NO as well as CO are convex functions of the equivalence ratio for lean combustion.

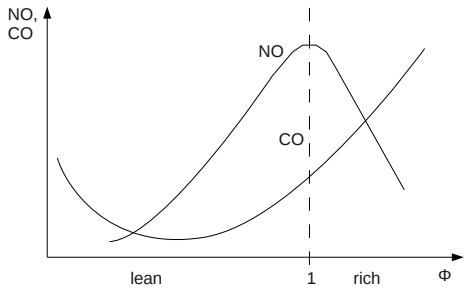

Figure 5: Qualitative behavior of NO and CO vs. equivalence ratio

Figures 6 and 7 show the influence of the forcing amplitudes respectively forcing frequencies on the emissions of CO and NO for laminar and turbulent cases. The values of the mass fractions of CO and NO for the particular cases are temporal averaged values taken at a position of 10 cm downstream of the mean flame position. Regarding the amplitude dependence in Fig. 6 it can be observed that for 30 Hz the emissions

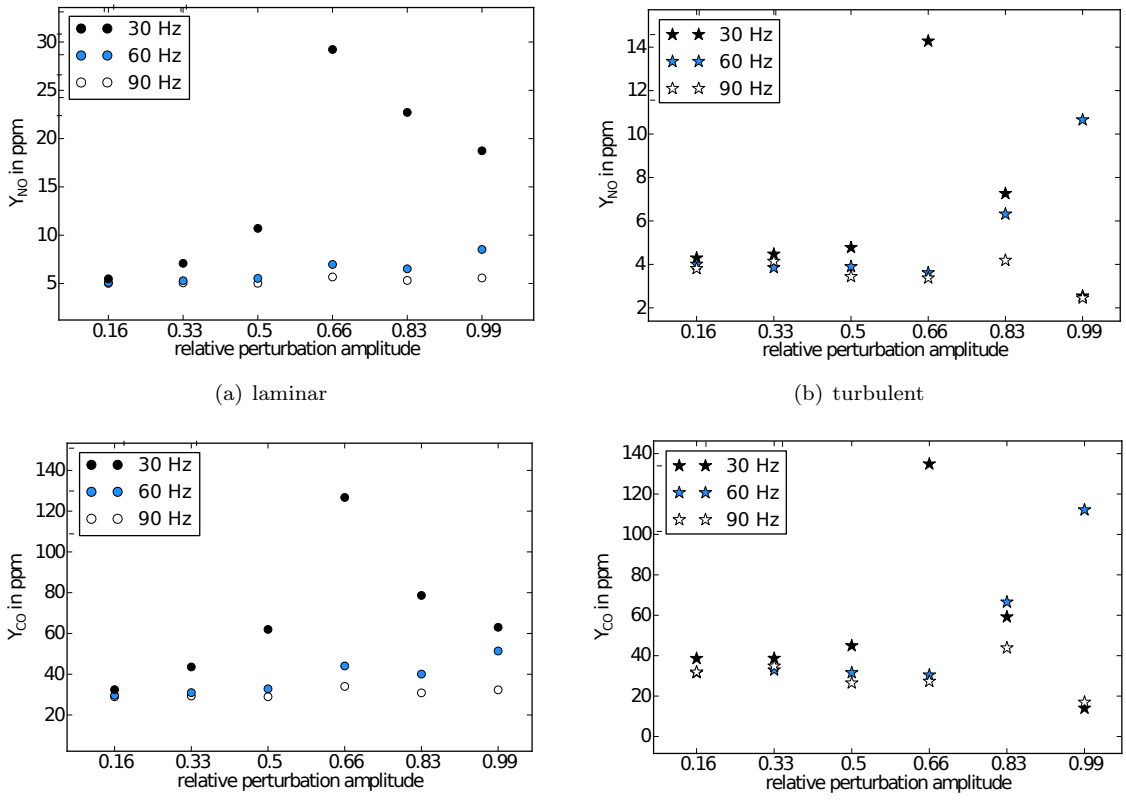

(a) laminar

(b) turbulent

(c) laminar

(d) turbulent

Figure 6: Influence of forcing amplitude on mean emissions of NO and CO. (a) Mean NO mass fraction, laminar; (b) mean NO mass fraction, turbulent; (c) mean CO mass fraction, laminar; (d) mean CO mass fraction, turbulent

increase with amplitude up to a relative perturbation amplitude of 0.66. This behavior can be explained by the convex dependence of NO and CO on the equivalence ratio. This causes higher mean values of the NO and CO-emissions subject to sinusoidal equivalence ratio oscillations than for the averaged steady state equivalence ratio. The increase of emissions is strongest for the forcing at 30 Hz since the highest amplitudes reach the flame here but is also present for 60 and slightly for 90 Hz. For higher amplitudes at 30 Hz the emissions decrease again for laminar as well as turbulent simulations. The behavior of NO and CO emissions is very similar. Comparing laminar and turbulent simulations the following differences can be found: For 30 Hz the increase in emissions is less distinct and the decrease for amplitudes higher than 0.66 is stronger for turbulent than laminar cases. The maximum NO emissions are higher for the laminar case whereas the maximum CO emissions of laminar and turbulent cases are comparable. For 60 Hz on the other hand the growth is stronger for turbulent simulations and no maximum is reached. For 90 Hz the influence of amplitude in the laminar case is negligible whereas the emissions increase in the turbulent case up to an amplitude of 0.83 and then decrease to a value lower than that without forcing.

The frequency dependence in Fig. 7 shows higher emissions for decreasing frequency. For the turbulent consideration and 20 Hz the emissions are again lower than for 30 Hz.

As already explained the increase of emissions can be related to the convex relation of NO- and CO-emissions on the equivalence ratio. The non-linear behavior, i.e. the adjacent decrease, can partly, for NO, be attributed to the dependence of NO emissions on the equivalence ratio. When forcing with a high enough amplitude NO would decrease again as the equivalence ratio extends into the rich combustion region. This

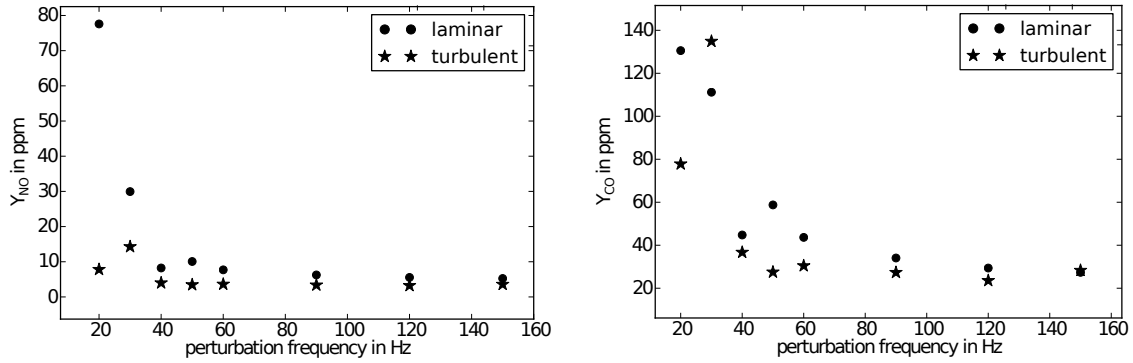

(a) (b)

Figure 7: Influence of forcing frequency on mean emissions of NO and CO at a relative forcing amplitude of 0.66. (a) Mean NO mass fraction; (a) mean CO mass fraction

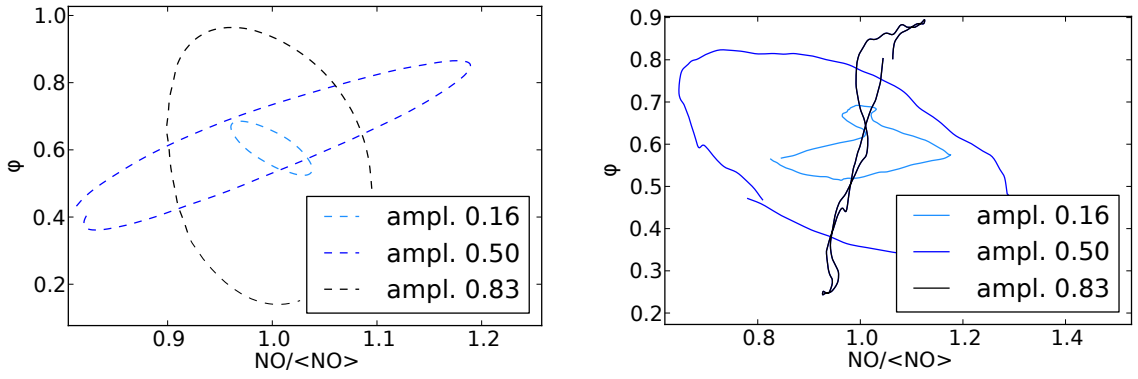

(a) laminar (b) turbulent

Figure 8: Phase averaged relation between NO fluctuations 10 cm downstream of the flame and equivalence ratio oscillations at the inlet for 30 Hz and different forcing amplitudes. (a) laminar; (b) turbulent.

is not the case for CO and also the amplitudes of oscillations at the flame front are for the most cases not high enough to attain the rich flame region. The effect seen here is caused by the complex interaction of the burning velocity and the oscillation in equivalence ratio. As mentioned in Sec. 3.2 the velocity and therefore the mass flow at the inlet is not constant since this corresponds to the concurrent burning velocity. This also results in a non-sinusoidal oscillation at the flame front. Depending on the phase between inflow equivalence ratio oscillation and burning velocity there are different consequences. There might be amplification or also damping. The present observations suggest a dampening effect for 30 Hz for amplitudes higher than 0.66 for both turbulent and laminar considerations and for 90 Hz for amplitudes higher than 0.83 for the turbulent case.

Figure 8 presents the phase averaged relation between NO fluctuations 10 cm downstream of the flame and equivalence ratio oscillations at the inlet for 30 Hz and different forcing amplitudes for laminar and turbulent simulations. The plots clearly show strongly varying behavior for the different amplitudes and the laminar and turbulent flames which implies different phase dependencies and concurs with the explanation given above.

3.4 Influence of equivalence ratio oscillations on heat release

The heat release rate and especially heat release fluctuations play an important role in gas turbines under combustion instabilities since they interact with pressure fluctuations and may enhance thermoacoustic instabilities under certain conditions.

Figure 9 shows the amplitude and frequency dependence of heat release fluctuations for laminar and turbulent simulations and in addition the influence of forcing amplitude on the mean heat release rate. The

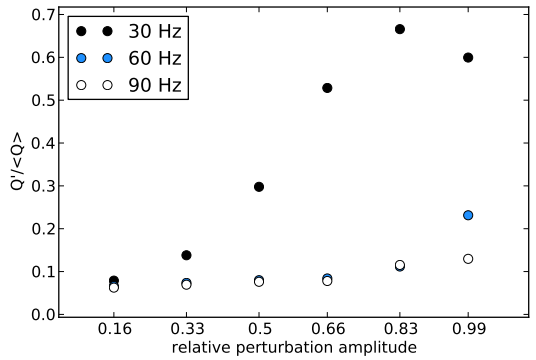

(a) Heat release fluctuation, laminar

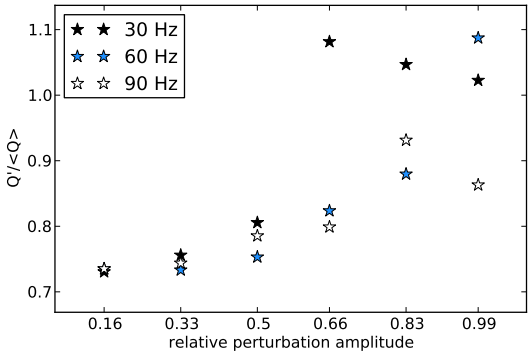

(b) Heat release fluctuation, turbulent

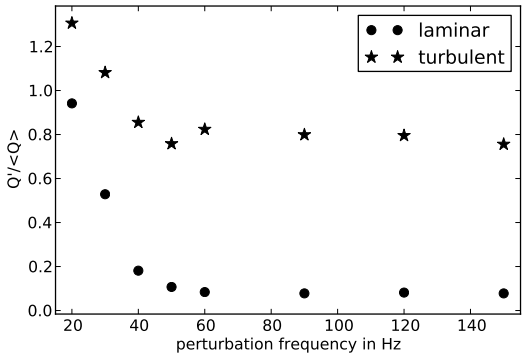

(c) Heat release fluctuation

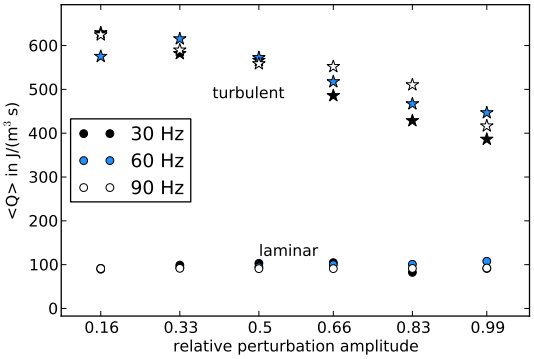

(d) Mean heat release rate

Figure 9: Amplitude and frequency dependence of the heat release fluctuations for laminar and turbulent simulations and the influence of forcing amplitude on the mean heat release rate (d).

heat release fluctuations for laminar and turbulent considerations show in general a similar behavior. For all frequencies an increase in fluctuation amplitude with forcing amplitude can be observed until a certain threshold. For 30 Hz saturation establishes at a relative perturbation amplitude between 0.66 and 0.83. For 60 Hz no saturation occurs whereas 90 Hz shows saturation for an amplitude of 0.99. For the turbulent cases the heat release fluctuation amplitude decreases again for 30 Hz for forcing amplitudes higher than 0.66 and for 90 Hz for forcing amplitudes higher than 0.99. For the laminar case the heat release fluctuation amplitude decreases only for 30 Hz for forcing amplitudes higher than 0.83. Fig. 9(c) presenting the frequency dependence for a relative perturbation amplitude of 0.66 reveals strong increase in heat release fluctuations for decreasing perturbation frequency. For frequencies higher than 60 Hz the influence of forcing is negligible. The main difference between the laminar and turbulent results is the absolute amplitude of fluctuation which is for the turbulent unforced case more than seven times higher than for the laminar unforced case. The impact of forcing on the heat release fluctuation is for low frequencies on the other hand much more distinct for the laminar than for the turbulent cases. The turbulent simulations exhibit heat release fluctuation of about 70% of the mean heat release for the unforced case which increase to values of more than 100% when forcing is applied.

Assuming constant oxidizer mass flow the heat release increases linearly with equivalence ratio for lean conditions. Close to stoichiometric and for rich conditions the heat release rate remains constant. This dependence implies saturation for high equivalence ratio oscillation amplitudes. The saturation and decreasing heat release fluctuations for very high forcing amplitudes can additionally, as already the behavior of NO and CO, be attributed to non-linear effects due to the interaction of burning velocity and equivalence ratio oscillations which overlay with the heat release-equivalence ratio-dependence saturation.

Regarding the mean heat release rate in Fig. 9(d) it is interesting to note that the mean heat release rate for the turbulent case decreases with amplitude for all considered frequencies. For the laminar case the mean heat release rate varies slightly but remains overall at similar values for all amplitudes and frequencies. The decreasing heat release rate for turbulent considerations is caused by decreasing mass flow rates which in turn are due to decreasing burning velocities which will be discussed in detail in Sec. 3.5.

3.5 Influence of equivalence ratio oscillations on burning velocity

The burning velocity is one of the most important parameters in premixed combustion. It couples directly with the flow field and perturbations of the equivalence ratio. For steady state considerations the displacement speeds (Equ. 14) for all species that play a role during the combustion process compare quantitatively well and correspond to the burning velocity. Regarding an unsteady problem this does not apply anymore. We will therefore regard displacement speeds of following species groups which exhibit similar behavior: reactants (O_2 + CH_4), products (CO_2 + H_2O) and intermediates (NO). The response of the mean displacement speed is again plotted against amplitude (Fig. 10, 11, and 13) and frequency (Fig. 14) for laminar and turbulent simulations. The displacement speeds are normalized by the unforced laminar respectively turbulent burning velocities, 0.22 m/s and 1.7 m/s.

The laminar case in Fig. 10(a) shows an increase of (O_2 + CH_4)-displacement speed with forcing amplitude which was expected as the oscillations were directly imposed on the methane and oxygen mass fractions. The turbulent case in Fig. 10(b) also shows a growth of (O_2 + CH_4)-displacement speed but only at an relative forcing amplitude of 0.99.

The influence of forcing on the displacement speed of CO_2 + H_2O (Fig. 11) is quite different for laminar and turbulent cases. The laminar results exhibit slight variations in displacement speeds with varying forcing amplitude but do not imply any distinct dependency. The turbulent results however show a decrease of displacement speed with increasing forcing amplitudes for all considered frequencies. As the averaged displacement speed of CO_2 and H_2O was taken as the inflow velocity this correlates with the mean mass flow rate and the mean heat release rate (Fig. 9(d)). The decrease of CO_2 and H_2O displacement speed with forcing amplitude can be explained by regarding the temporal evolution of the displacement speed of CH_4 and CO_2 for different forcing amplitudes (Fig. 12). For low forcing amplitudes (Fig. 12(a)) no distinct periodic but only stochastic behavior can be observed. The time history for the different species agrees well. For the higher forcing amplitude (Fig. 12(b)) periodic patterns are present in the time history of the displacement speeds. It can be clearly seen that at minima of the oscillations turbulent fluctuations in the displacement speeds are suppressed. For low values of methane that is for very lean conditions the reaction zone broadens

and property gradients become smaller. For small gradients turbulent eddies have less influence and therefore fluctuations are damped. This damping occurs for all species and is also the reason that growth of the mean O_2- and CH_4-displacement speeds only occurs for very high forcing amplitudes.

Considering the normalized mean displacement speed for NO (Fig. 13) the laminar results show an increase with relative perturbation amplitude with saturation at very high forcing amplitudes. This is again caused by the convex dependence of NO on the equivalence ratio (see Sec. 3.3). The turbulent results indicate a superposition of the laminar behavior with the damping of the turbulent fluctuations.

The frequency dependence of the different groups of displacement speed at a relative forcing amplitude of 0.66 is given in Fig. 14. For the laminar considerations the displacement speed of NO strongly increases with decreasing frequencies whereas the displacement speed of CO_2 + H_2O and O_2 + CH_4 do not show major effects. The turbulent results indicate a slight increase in displacement speed of NO and an in comparison stronger decrease in displacement speeds of CO_2 + H_2O and O_2 + CH_4. The characteristics of the displacement speeds of CO_2 + H_2O and O_2 + CH_4 compare very well for all considered conditions whereas the absolute value for the displacement speeds of O_2 + CH_4 are slightly higher than those of CO_2 + H_2O. The frequency dependence suits the explanations given before.

Figure 15 shows the relative displacement speed fluctuations for 30 Hz plotted against forcing amplitude. The plots give the dependencies for the different displacement speed groups and for laminar and turbulent considerations. As already for the mean results the fuctuations of the different groups feature different behavior. The CO_2 + H_2O-displacement speed fluctuations show characteristics similar to those of the heat

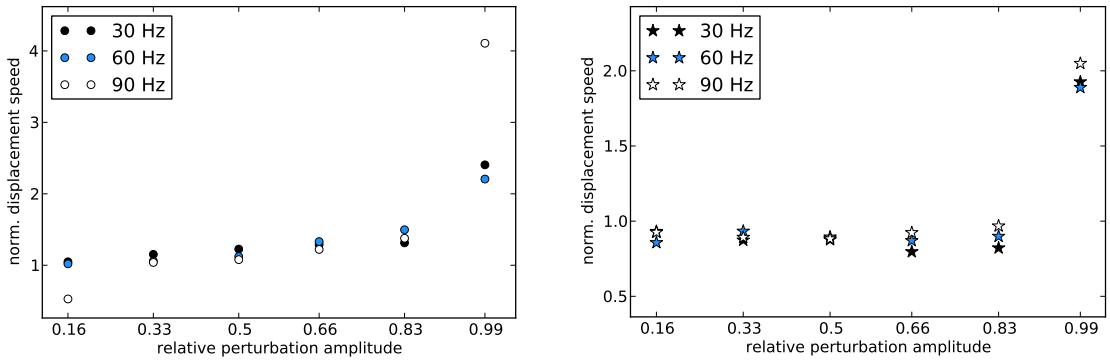

(a) Laminar (b) Turbulent

Figure 10: Displacement speeds for CH_4 and O_2, averaged, for different forcing amplitudes and frequencies, normalized by the unforced burning velocity.

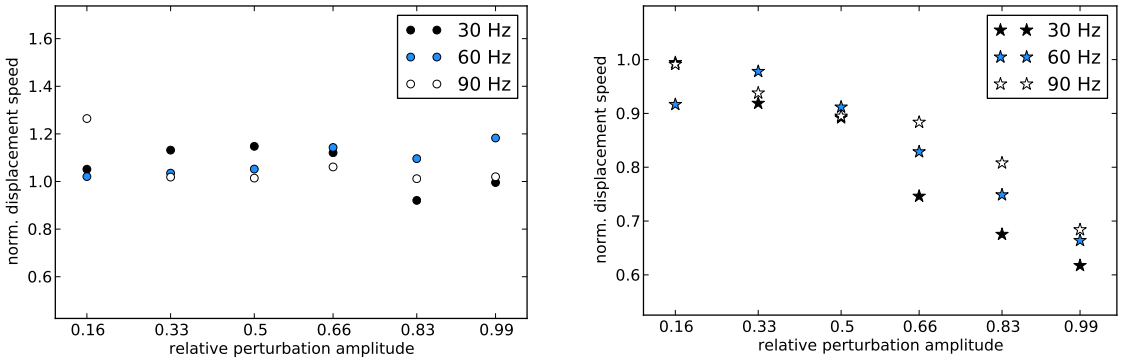

(a) Laminar (b) Turbulent

Figure 11: Displacement speeds for CO_2 and H_2O, averaged, for different forcing amplitudes and frequencies, normalized by the unforced burning velocities.

release fluctuations. The fluctuations grow up to a relative perturbation amplitude of 0.66 and 0.83 for

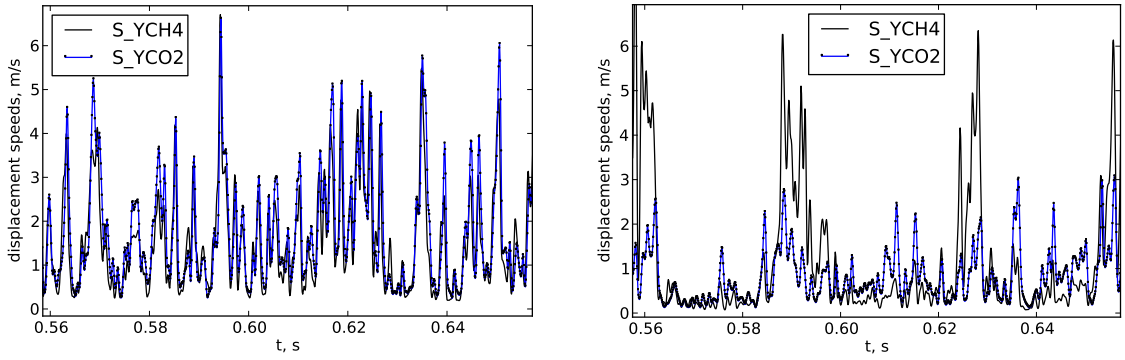

(a) (b)

Figure 12: Time history of CH_4 and CO_2 displacement speeds at 30 Hz. (a) relative forcing amplitude of 0.16; (b) relative forcing amplitude of 0.83

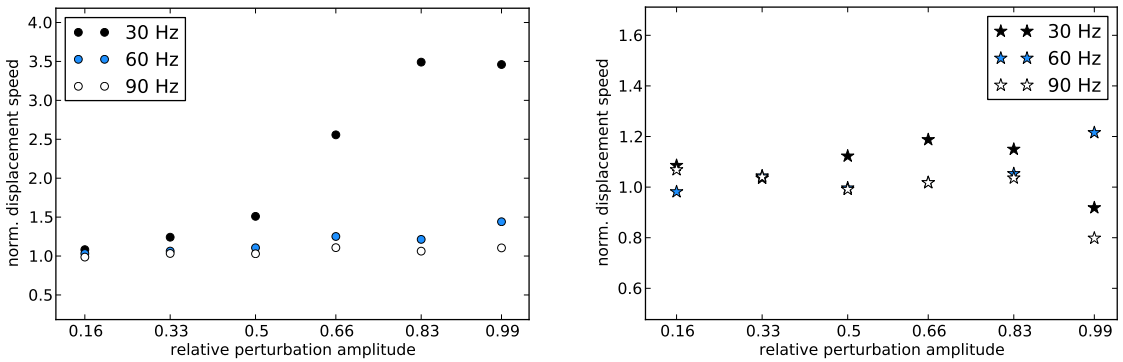

(a) Laminar (b) Turbulent

Figure 13: Displacement speeds for NO for different forcing amplitudes and frequencies, normalized by the unforced burning velocities.

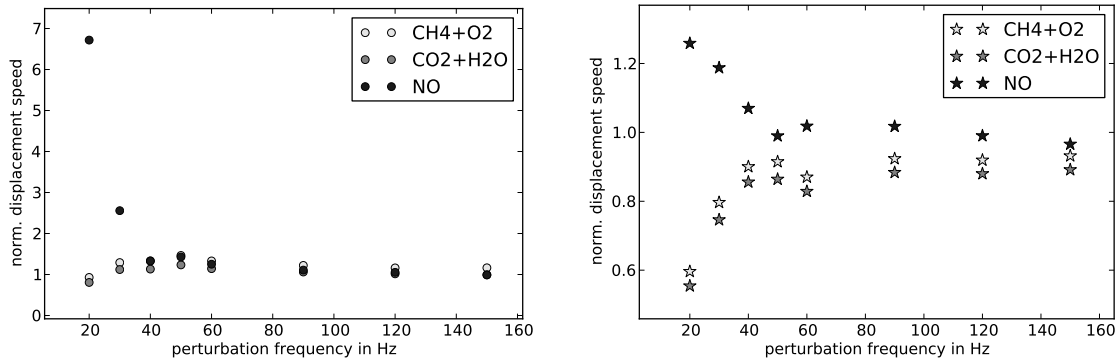

(a) Laminar (b) Turbulent

Figure 14: Displacement speeds for different forcing frequencies, divided into CH4 + O2, CO + H2O, and NO, normalized by the unforced burning velocities.

laminar respectively turbulent simulations and decay for higher amplitudes. The NO-displacement speed fluctuations show similar trends but are generally higher than the CO_2 + H_2O-displacement speed fluctuations. The mechanisms behind the saturation process are similar to that of the heat release fluctuations. On the one hand saturation due to extension in stoichiometric and rich flame regions takes place where the burning velocity has its maximum and decreases again and on the other hand non-linear effects caused by the interaction of inflow velocity and equivalence ratio fluctuations superimpose. The O_2 + CH_4-displacement speed fluctuations directly depend on the equivalence ratio oscillations and therefore do not show saturation effects.

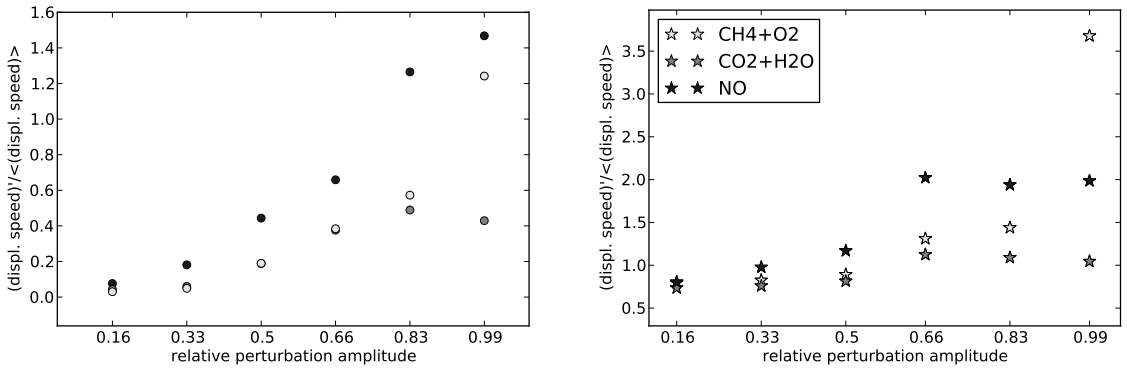

(a) Laminar

(b) Turbulent

Figure 15: Displacement speed fluctuations for different forcing amplitudes for 30 Hz, divided into CH4 + O2, CO + H2O, and NO

4 Conclusion

The present studies investigate the influence of equivalence ratio oscillations on flame characteristics for lean partially-premixed laminar and turbulent one-dimensional flames. The flame response was characterized by evaluating the NO and CO emissions, the heat release fluctuations, and the displacement speeds in dependence on forcing frequencies and amplitudes. The inflow velocity was set to the instantaneous burning velocity. It was found that emissions of NO as well as CO increase with forcing amplitude up to a certain value of forcing amplitude. This behavior correlates with the convex relation of NO and CO on the equivalence ratio. Laminar and turbulent simulations show the same tendencies although differences in absolute values and in the frequency dependence are present. Decreased NO and CO emissions for higher forcing amplitudes were explained by the complex interaction of burning velocity with equivalence ratio oscillation leading to non-linear effects. Fluctuations in the heat release rate exhibit an increase with amplitude and saturation for certain frequencies which are attributed to equivalence ratio dependecies and the same non-linear effects as for the emissions. The mean displacement speeds were considered separately for reactants, products and the intermediate species NO. Quite different behavior is observed for the different groups. For the laminar case an increase of the reactants displacement speed, no distinct behavior for the products displacement speed and an increase in NO-displacement speed is found. The turbulent considerations expose damping of turbulent fluctuations in the displacement speed when forcing is applied which becomes more distinct with higher forcing amplitudes and lower forcing frequencies. This damping leads to a decrease of displacement speeds which superposes on the characteristics found for the laminar case. The burning velocity therefore decreases with forcing amplitude for the turbulent case which also results in decreasing mean heat release rates.

References

[1] Ying Huang and Vigor Yang. Dynamics and stability of lean-premixed swirl-stabilized combustion. *Progress in Energy and Combustion Science*, 35:293–364, 2009.

[2] C. O. Paschereit, E. J. Gutmark, and W. Weisenstein. Coherent structures in swirling flows and their role in acoustic combustion control. *Physics of Fluids*, 11(9):2667–2678, 1999.

[3] C. O. Paschereit, , E. J. Gutmark, and W. Weisenstein. Excitation of Thermoacoustic Instabilities by Interaction of Acoustics and Unstable Swirling Flow. *AIAA Journal*, 38(6):1025–1034, 2000.

[4] THIERRY POINSOT and SEBASTIEN M. CANDEL. A Nonlinear Model for Ducted Flame Combustion Instabilities. *Combustion Science and Technology*, 61(4-6):121–153, 1988.

[5] T. Lieuwen and B. T. Zinn. The role of equivalence ratio oscillations in driving combustion instabilities in low NOx gas turbines. In *27th Symposium (International) on Combustion/The Combustion Institute*, pages pp 1809–1816, 1998.

[6] T. Lieuwen, Y. Neumeier, and B. T. Zinn. The Role of Unmixedness and Chemical Kinetics in Driving Combustion Instabilities in Leam Premixed Combustors. *Combustion Science and Technology*, 135:193–211, 1998.

[7] Ramanan Sankaran and Hong G. Im. Dynamic Flammability Limits of Methane/Air Premixed Flames with Mixture Composition Fluctuations. *Proceedings of the Combustion Institute*, 29(1):77 – 84, 2002.

[8] Ju Hyeong Cho and Tim Lieuwen. Laminar premixed flame response to equivalence ratio oscillations. *Combustion and Flame*, 140(1-2):116 – 129, 2005.

[9] K. König, B. Bykov, and U. Maas. Investigation of the dynamical response of methane-air counterflow flames to inflow mixture composition and flow field perturbations. *Flow, Turbulence and Combustions*, 2008.

[10] Shreekrishna, Santosh Hemchandra, and Tim Lieuwen. Premixed flame response to equivalence ratio perturbations. *Combustion Theory and Modelling*, 14(5):681–714, 2010.

[11] E. S. Richardson, V. E. Granet, A. Eyssartier, and J. H. Chen. Effects of equivalence ratio variation on lean, stratified methane-air laminar counterflow flames. *Combustion Theory and Modelling*, 14(6):775–792, 2010.

[12] R. Rhou and S. Hochgreb. The Behaviour of Laminar Stratified Methaine/Air Flames in Counterflow. *Preprint submitted to Combustion and Flame*, 2012.

[13] R. Balachandran, A.P. Dowling, and E. Mastorakos. Response of turbulent premixed flames subjected to inlet velocity and equivalence ratio perturbations. In *Proceeding of the European Combustion Meeting*, 2005.

[14] A.L. Birbaud, S. Ducruix, D. Durox, and S. Candel. The nonlinear response of inverted "v" flames to equivalence ratio nonuniformities. *Combustion and Flame*, 154(3):356 – 367, 2008.

[15] R. Balachandran, A.P. Dowling, and E. Mastorakos. Dynamics of bluff-body stabilised flames subjected to equivalence ratio oscillations. In *Proceeding of the European Combustion Meeting*, 2011.

[16] Kyu Tae Kim, Jong Guen Lee, Bryan D. Quay, and Domenic A. Santavicca. Experimental Investigation of the Nonlinear Response of Swirl Stabilized Flames to Equivalence Ratio Oscillations. *Journal of Engineering for Gas Turbine and Power*, 133(43970):833–842, 2011.

[17] R. S. Barlow and J.-Y. Chen. On Transient Flamelets and their Relationship to Turbulent Methane-Air Jet Flames. *Twenty-Fourth Symposium (International) on Combustion/The Combustion Institute*, pages 231–237, 1992.

[18] Hong G Im, Jacqueline H Chen, and Jyh-Yuan Chen. Chemical Response of Methane/Air Diffusion Flames to Unsteady Strain Rate. *Combustion and Flame*, 118(1Ũ2):204 – 212, 1999.

[19] Vito S Santoro, Dimitrios C Kyritsis, Mitchell D Smooke, and Alessandro Gomez. Nitric Oxide Formation during Flame/Vortex Interaction. *Proceedings of the Combustion Institute*, 29(2):2227–2233, 2002.

[20] Alan R. Kerstein. Linear-eddy modeling of turbulent transport. II: Application to shear layer mixing. *Combustion and Flame*, 75(3-4):397–413, 1989.

[21] Alan R. Kerstein. Linear-eddy modelling of turbulent transport. Part6 Microstructure of diffusive mixing fields. *J. Fluid Mech.*, 231:361–394, 1991.

[22] J. Warnatz, U. Maas, and R.W. Dibble. *Combustion*. Springer, 4th edition, 2006.

[23] Thomas Smith and Suresh Menon. Model simulations of freely propagating turbulent premixed flames.

Symposium (International) on Combustion, 26(1):299 – 306, 1996.

[24] S. Menon, M. A. McMurtry, A. R. Kerstein, and J. Y. Chen. Prediction of NOx production in a turbulent hydrogen-air jet flame. *Journal of Propulsion and Power*, 10:161–168, 1994.

[25] D. Lignell, A. Kerstein, G. Sun, and E. Monson. Mesh adaption for efficient multiscale implementation of one-dimensional turbulence. *Theoretical and Computational Fluid Dynamics*, pages 1–23, 2012. 10.1007/s00162-012-0267-9.

[26] Tarek Echekki, Alan R. Kerstein, and James C. Sutherland. *Turbulent Combustion Modeling: Advances, New Trends and Perspectives*, volume 95 of *Fluid Mechanics and Its Applications*, chapter 11 The One-Dimensional-Turbulence Model, pages 249–276. Springer, 1st edition, 2011.

[27] S. D. Cohen and A. C.Hindmarsch. CVODE, a Stiff/Nonstiff ODE Solver in C. *Computers in Physics*, 10(2):138–143, 1996.

[28] M. Oevermann, H. Schmidt, and A.R. Kerstein. Investigation of Autoignition under Thermal Stratification using Linear Eddy Modeling. *Combustion and Flame*, 155:370–379, 2008.

[29] Gregory P. Smith, David M. Golden, Michael Frenklach, Nigel W. Moriarty, Boris Eiteneer, Mikhail Goldenberg, C. Thomas Bowman, Ronald K. Hanson, Soonho Song, William C. Gardiner Jr., Vitali V. Lissianski, and Zhiwei Q. GRI-Mech 3.0, The Gas Research Institute. `http://www.me.berkeley.edu/gri-mech/`.

[30] Abu-Orf, G.M., Cant, and R.S. Reaction rate modelling for premixed turbulent methane-air flames. In *Joint Meeting of the Portuguese and British and Spanish and Swedish Sections of the Combustion Institute and 1-4 April 1996 and Madeira and Portugal.*

[31] D. Goodwin. Cantera: An object-oriented software toolkit for chemical kinetics, thermodynamics, and transport processes. http://code.google.com/p/cantera, 2009.

[32] N. PETERS. Local quenching due to flame stretch and non-premixed turbulent combustion. *Combustion Science and Technology*, 30(1-6):1–17, 1983.